Kilometer scale Kaiser-effect identified in Krafla volcano, Iceland

Elías Rafn Heimisson[1] Páll Einarsson[1] Freysteinn Sigmundsson[1] Bryndís Brandsdóttir[1]

Corresponding author: E. R. Heimisson, Department of Geophysics, Stanford University, Mitchell Building, 397 Panama Mall, Stanford, CA 94305 (eliasrh@stanford.edu)

[1]Nordic Volcanological Center, Institute of Earth Sciences, University of Iceland, IS-101 Reykjavik, Iceland.

The Krafla rifting episode in 1975–1984, consisted of around 20 inflation-deflation events within the Krafla caldera, where magma accumulated during inflation periods and was intruded into the transecting fissure swarm during brief periods of deflation. We re-analyse geodetic and seismic data from the rifting episode and perform a time-dependent inversion of a leveling time-series for a spherical point source in an elastic half-space. Using the volume change as a proxy for stress shows that during inflation periods the seismicity rate remains low until the maximum inflation of previous cycles is exceeded thus exhibiting the Kaiser effect. Our observations demonstrate that this phenomenon, commonly observed in small-scale experiments, is also produced in kilometer-scale volcanic deformation. This behavior sheds new light on the relationship between deformation and seismicity of a deforming volcano. As a consequence of the Kaiser effect, a volcano may inflate rapidly without significant changes in seismicity rate.

1. Introduction

A common practice in geoscience is to apply observed small-scale processes or measured parameters in the laboratory to large-scale processes. The assumption that small-scale experiments apply to kilometer-scale processes of the earth is, however, difficult to verify. In some cases discrepancies have been demonstrated, for example, by showing the kilometer scale tensile strength of granite was up to an order of magnitude smaller than the typical laboratory values [*Jónsson*, 2012].

Loading of many rock types, and other materials, produces acoustic emissions (AE) that are easily measurable in a laboratory. AE are often used as a proxy for the nucleation and growth of microcracks in deforming rocks. Under cyclic loading and unloading, however, some materials produce little or no AE until the stress of the previous cycle is exceeded. This is referred to as the Kaiser "stress memory" effect [*Kaiser*, 1953]. At that point the material produces a dramatic increase in AE [*Lockner*, 1993]. The best understood and established manifestation of the Kaiser effect occurs under uni-axial compression where the Kaiser effect can be used to measure the previous maximum loading of the material. The Kaiser effect can thus be used as a measure of compressive stress. However, various complications in rock mechanics need to be considered, for example, healing of microfactures with time, which can cause the increase in AE at lower stresses [*Lavrov*, 2003]. The Kaiser effect has been shown to occur in many rock types and has been suggested as a way to measure *in-situ* stresses, thus with possible application to many geological processes [*Li and Nordlund*, 1993]. Furthermore, the Kaiser effect has been verified experimentally on samples of volcanic rocks from Mt. Etna volcano and the results interpreted with respect to seismicity and deformation of Etna [*Heap et al.*, 2009].

Even though the Kaiser effect is relatively well documented for volcanic rock samples in laboratory settings, it has not been shown to be present in a volcanic setting on a kilometer scale. A few studies exist that associate the Kaiser effect with patterns in seismicity caused by induced pore-pressure changes from water table variations of lakes and reservoirs [*Simpson and Negmatullaev*, 1981] or fluid–injection [*Baisch et al.*, 2009]. As pointed out in a 2003 review on the Kaiser effect by *Lavrov* [2003], the manifestation of stress memory on a large scale is unclear and requires more research.

In a volcanic setting perhaps the most obvious case of cyclic stressing is during inflation and deflation of a magma chamber. Cyclic inflation and deflation was observed during the rifting episode of 1975–1989 at Krafla in Iceland (Figure 1) during which magma accumulated continuously within a shallow-level magma chamber and was injected into the adjacent rift shortly after the chamber pressure exceeded a threshold value, altogether 20 times [*Björnsson et al.*, 1977, 1979; *Buck et al.*, 2006]. Cyclic inflation and deflation has also been observed at other volcanoes, including Piton de La Fournaise [*Peltier et al.*, 2008], Etna [*Bruno et al.*, 2012] and Soufriere Hills [*Voight et al.*, 1998]. If we assume that the magma chamber inflation can be approximated by spherical point source in an elastic half-space then the stress tensor in the surrounding crust can be calculated using solutions provided by *Okada* [1992]. By calculating the stress tensor at multiple points in a dense grid surround a inflation source we found that although the crust undergoes net dilatation the change in the most compressive principal stress σ_1 is nevertheless compressive or very close to zero. Cyclic compression along σ_1-axis can therefore be expected in the vicinity of the magma chamber and theoretically such system could manifest the Kaiser effect. However, this theory requires observational confirmation which we present in this study. Confirmation of the occurrence of the Kaiser effect in active volcanoes sheds light on scale dependence of stress memory in volcanic rocks and the relationship between seismicity and deformation during volcanic unrest.

2. Data and Methods

During the Krafla rifting episode, regular leveling surveys were carried out in the area of greatest deformation. A spatial and temporal interpolation was carried out by [*Björnsson and Eysteinsson*, 1998] on 87 stations (Figure 1c). The mean number of observations for the stations was 25 for the period from 1975 to 1995. Measurements were most frequent in the period of most rapid changes in deformation. The temporal interpolation was based on daily tilt measurements at one site and performed on the observed elevations and the elevation values estimated with the spatial interpolation of the 87 stations. This provided a 2600 step time-series for each station. We took those stations and performed a time-dependent inversion at each time-step. Figure 2 shows an example of a time-series from the benchmark FM5596, where maximum vertical movements were observed. A simple Mogi source [*Mogi*, 1958] fits the leveling data reasonably well, providing a time history of the volume change, which we regard as a measure of state of stress in the crust.

The earthquake count is not as complete as the leveling data because while most dikes travelled north from the center of inflation within the Krafla caldera some propagated to the south. During the rifting episode there were two periods where dikes propagated to the south, first in April and September 1977 and second in February and March 1980 [*Einarsson*, 1991; *Björnsson and Eysteinsson*, 1998]. Because the dikes had long-lived aftershock activity, it wasn't always possible to distinguish earthquakes due to caldera inflation from events originating in the dikes. This wasn't a problem in periods where all dikes propagated to the north since the seismic station used for the counting was located south of the caldera and thus not sensitive to the decaying seismicity of the northern dikes. As a result, the seismicity count data is missing from the two periods where dikes propagated to the south. Located events are much fewer than counted earthquakes, they however reflect the geometric distribution of the seismic activity during inflation periods (Figure 1b). All events with an amplitude of more than 5 mm on the trace at the Reynihlíð seismic station (black triangle on Figure 1c) were counted, most of which much too small to be located or detected on other seismic stations. The inflation seismicity rate was published in part by *Björnsson et al.* [1977].

For the inversion of the leveling data, each time-series was referenced to the date elevation of the point with the minimum value at benchmark FM5596 (Figure 2). That day was assumed to have no vertical displacement and thus the volume change of the Mogi source was assumed to be zero. At each time step a simulated annealing algorithm [*Cervelli et al.*, 2001] is used to minimize a misfit function:

$$\chi^2 = \sum_{i=1}^{87} = \frac{(u_i^{\text{pre}} - u_i^{\text{obs}})^2}{\sigma_i^2} \tag{1}$$

where u_i^{pre} and u_i^{obs} are the model predicted and observed vertical displacements at the i-th benchmark, σ_i is the error of u_i^{obs}. *Björnsson et al.* [1985] estimate there to be two main sources of error. The first error source was a systematic error of 0.05 mm per meter of elevation difference between the i-th benchmark and the reference benchmark Kóngspunktur, located near the Reynihlíð seismic station (Figure 1c). The second main error source was an internal measurement error which was estimated to be 5.5 mm between Kóngspunktur and FM5596, and assumed constant on all benchmarks. The error is propagated to the model parameters by a bootstrap method [*Efron and Tibshirani*, 1986] where we randomly sample the data vector within the ranges of the aforementioned estimated error. Then the inversion is repeated. The easting and northing location and the depth of the source at each time step all prove to be stable both with 2σ error usually less than 40 m in easting, northing and depth location. The simulated annealing method was followed by a derivative-based minimization method to ensure a minimum was reached. The optimization scheme applied here consistently converged to the same minimum.

3. Results

The mean location of the source throughout the time period was at 65.7099°N, -16.7575°E and mean depth of the source was 4.3 km. By calculating the standard deviation of all 2600 time steps, the best-fitting model gave 2σ value: 1 km in easting and depth locations and 1.2 km in northing location. This shows that the source center was usually located within a sphere of 1 km radius and thus relatively steady with time from 1975 to 1995. For the first four cycles of inflation and deflation, the simple Mogi model provides a good fit to the data (Figure 3). Following the southward migrating dike of late April 1977, which erupted inside the caldera, a significant signal from the eruptive fissure formation contaminated the leveling time-series. However, the deformation due to the magma chamber was so large that the inversion nevertheless returns a rather stable source throughout the time-series. The inversion results indicated that the source center started at around 3–4 km depth but then migrated deeper and by 1978 became stable at around 4.5 km (Figure S1 in Supplementary Information). Single sphere modelling of individual inflation periods by *Ewart et al.* [1991], using distance, tilt and levelling measurements, suggested the source depth to be generally in the range 3–4 km and the inflation periods in 1981 and 1983 came out with significantly greater depth at around 4.5–5.0 km. This is in reasonable agreement with our results. However, our model is only constrained by vertical displacement and may thus give rather poor constrains on depth. There was also slight systematic shift in the location of the source with time in longitude (Figure S2 in Supplementary Information).

A comparison of the volume change with the rate of caldera earthquakes reveals the occurrence of a large-scale Kaiser effect (Figure 4). The rate of seismicity correlates well with the inflation during the first inflation period. In subsequent cycles the seismicity is very low until the maximum inflation level of the previous cycle is exceeded and an abrupt increase in seismicity is observed, reaching similar rate as before the deflation. The first three cycles of inflation/deflation (Figure 4a) clearly demonstrate the Kaiser effect. The seismicity rate remains at rather low levels for two inflation/deflation cycles (Figure 4b), in agreement with the previous cycle having reached higher level of inflation than the subsequent two cycles. At least six dikes had been produced prior to January 1978 (Figure 4b) some of which erupted inside the caldera [*Einarsson*, 1991]. This undoubtedly altered the stress field inside the caldera, due to the high sensitivity of the Kaiser effect to rotation of the principal axes [*Lavrov*, 2003], we might thus expect the Kaiser effect to have been moved toward lower stress, thus occurring at less volume, or maybe even higher stresses. However the Kaiser effect still occurs in good agreement with the inflation of previous periods (Figure 4b). Note that the scale on the seismicity rate is different between Figures 4a and 4b suggesting that the mean seismicity rate is decaying with greater inflation. The 1981-1985 period (Figure 4c) is characterized by inflation with less volumetric inflow than before and thus lower stressing rate. At this point the Kaiser effect does not appear to be present. There are some bursts of increased seismicity rate which do not seem to show an agreement with inflation exceeding the previous stages, although some spikes correlate with periods of higher inflow and thus increased stressing rate. However, in the period preceding 1981 at least 14 dikes were produced, 7 of which lead to eruptions [*Buck et al.*, 2006]. We thus expect the stress field would have been altered greatly and the manifestation of the Kaiser effect as well.

4. Discussion

Based on the leveling time-series (Figure 2), the Krafla volcano appears to have been in an inflated state before the first diking event. Few geophysical observations exist prior to the first diking event and the leveling data has in fact only one observation pre-dating the initial diking event. It is, therefore, difficult to conclude how rapidly or even if the volcano inflated significantly prior to the initial diking. However, increased seismic activity was observed within the caldera during 1975, prior to the initial deflation and diking event in December 1975. It is noteworthy that, the first dike caused deflation of the caldera with a maximum subsidence in the caldera of about 2 m. This is around twice the deflation caused by the second greatest deflation event of the rifting episode. The caldera inflation ceased in 1989 with the volcano in an inflated state. A slow subsidence has been recorded since, most likely caused by plate spreading and cooling of the crust in response to geothermal exploitation by the Krafla power plant, located within the caldera [*Sturkell et al.*, 2008; *Ali et al.*, 2014].

The level of inflation within the caldera prior to the first diking event was higher than during the following 6 inflation/deflation cycles (Figure 2). It is therefore logical to ask why the threshold stress for the Kaiser effect is not at the inflation state before the first dike. One might expect that no significant seismicity rate should be present until after the inflation exceeds the pre-diking state. As was noted before, the volcano exhibited unusually large deflation signal during the first dike, suggesting very high pressure in the magma chamber. This indicates that the state of stress in the crust surrounding the magma chamber might have been close to the material strength. If the preloading compression of a brittle rock reaches higher than about 80% of the ultimate strength, the Kaiser effect will typically move toward lower stress in the next stressing cycles [*Lavrov*, 2003]. It may also be significant that the initial deflation of the caldera lasting from December 1975 to March 1976 was accompanied by considerable seismic activity. At least three earthquakes of magnitude 5 occurred within the caldera during its subsidence [*Einarsson*, 1986]. This seismic activity is likely to have significantly altered the stress field around the magma chamber thus changing the manifestation of the Kaiser effect. Another explanation could simply be the time scale of the preloading. At the end of the Krafla rifting episode the inflation ceased in an inflated state. Presumably that might have also been the case for the last rifting episode in the Krafla system, the Mývatn Fires in 1724–1729 [*Sigmundsson*, 2006]. The Kaiser effect is sensitive to the duration of the preloading and the Kaiser effect decays faster if the preloading is close to the ultimate strength [*Lavrov*, 2003]. Assuming that the preloading lasted since the Mývatn Fires, it may have been long preloading duration, high preloading stress and stress field changes due to large earthquakes that all resulted in the Kaiser effect not being present during the first reloading cycle.

As noted before, the manifestation of the Kaiser effect was disturbed during the 1981-1985 period (Figure 4c), most likely caused by changes in the stress field. Loading rate may, however, also be a factor that influences the Kaiser effect. By rapidly reloading a rock the Kaiser effect may occur at lower stresses [*Lavrov*, 2003]. While this can be easily measured in the laboratory it is uncertain how rapid loading is required on kilometer-scale to produce the same effect. In our data, there is little evidence that rapid loading rate altered the manifestation of the Kaiser effect at Krafla. Near the end of the rifting episode, when the Kaiser effect had been disturbed, the volume change rate was lower than during earlier parts of the rifting episode.

The occurrence of the Kaiser effect during cyclic inflation/deflation of a volcano has important consequences for volcano monitoring and eruption forecasting. Imagine a scenario where a volcano, not monitored by geodetic measurement, shows signs of unrest through increased seismic activity and eventually erupts. A period of low seismicity following an eruption could follow, despite rapid inflation, if the volcano exhibits the Kaiser effect. Lack of seismicity, in absence of geodetic measurements, can therefore be misinterpreted as reflecting stable and safe conditions, with serious implications for risk evaluation. If that volcano fulfills the requirements for its eruptions to be inflation predictable [*Segall*, 2013] then, as a consequence of the Kaiser effect, seismic activity might not become unusual until a dike starts propagating away from a magma chamber. It is, therefore, clear that monitoring a volcano only with seismic observations is insufficient and complimentary geodetic observations are needed to properly understand hazards and risks in volcanic areas.

5. Conclusions

Although the Kaiser effect remains rather poorly understood in large-scale natural processes and under triaxial stressing [*Lavrov*, 2003], our results show its manifestation during cyclic stress loading and unloading of the crust in relation to magma flow in and out of a magma chamber. Even after at least 10 diking events and consequent perturbations to the stress field, the Kaiser effect could still be identified and occurred when the inflation of the previous cycle had been exceeded. Following the fourteenth dike on 18 November 1981 the seismicity stopped behaving in accordance with the Kaiser effect. Our results stress the importance of combining geodetic data with seismic data when monitoring volcanoes. A volcano in a cyclic inflation/deflation mode may not show abnormal seismicity until it is very close to an eruption. The Kaiser effect should thus be considered in interpretation of data for eruption forecasting and hazard assessment.

6. Acknowledgements

We thank all the many individuals involved in gathering data and monitoring during the Krafla rifting episode. Suggestions by Paul Segall and Jeffrey A. Karson helped improve this work. We thank Mike Heap and an anonymous reviewer for their excellent and constructive reviews of this paper. Support for this work was received from the European Community's Seventh Framework Programme Grant No. 308377 (Project FUTUREVOLC). Some figures were produced using the GMT public domain software. This paper is dedicated to the memory of Ármann Pétursson, the attendant of the seismic station in Reynihlíð, who passed away in 2012.

References

Ali, S. T., K. L. Feigl, B. B. Carr, T. Masterlark, and F. Sigmundsson (2014), Geodetic measurements and numerical models of rifting in Northern Iceland for 1993–2008, *Geophysical Journal International*, *196*(3), 1267–1280, doi:10.1093/gji/ggt462.

Baisch, S., R. Vörös, R. Weidler, and D. Wyborn (2009), Investigation of fault mechanisms during geothermal reservoir stimulation experiments in the Cooper Basin, Australia, *Bulletin of the Seismological Society of America*, *99*(1), 148–158, doi:10.1785/0120080055.

Björnsson, A., and H. Eysteinsson (1998), Breytingar á landhæð við Kröflu 1974-1995: samantekt á landhæðarmælingum: samvinnuverk Orkustofnunar, Norrænu eldfjallastöðvarinnar og Landsvirkjunar (in Icelandic), *Tech. rep.*, OS-98002, National Energy Authority Report, Reykjavik, Iceland.

Björnsson, A., K. Sæmundsson, P. Einarsson, E. Tryggvason, and K. Grönvold (1977), Current rifting episode in north Iceland, *Nature*, *266*(5600), 318–323, doi:10.1038/266318a0.

Björnsson, A., G. Johnsen, S. Sigurðsson, G. Thorbergsson, and E. Tryggvason (1979), Rifting of the plate boundary in North Iceland 1975–1978, *J. geophys. Res*, *84*(86), 3029–3038.

Björnsson, A., G. Björnsson, A. Gunnarsson, and G. Thorbergsson (1985), Breytingar á landhæð vid Kröflu 1974–1984 (in Icelandic), *Tech. rep.*, OS-85019/JHD-05, National Energy Authority Report, Reykjavik, Iceland.

Bruno, V., M. Mattia, M. Aloisi, M. Palano, F. Cannavò, and W. E. Holt (2012), Ground deformations and volcanic processes as imaged by CGPS data at Mt. Etna (Italy) between 2003 and 2008, *Journal of Geophysical Research: Solid Earth*, *117*(B7), doi:10.1029/2011JB009114, b07208.

Buck, W. R., P. Einarsson, and B. Brandsdóttir (2006), Tectonic stress and magma chamber size as controls on dike propagation: Constraints from the 1975-1984 Krafla rifting episode, *Journal of Geophysical Research: Solid Earth*, *111*(B12), doi:10.1029/2005JB003879, b12404.

Cervelli, P., M. H. Murray, P. Segall, Y. Aoki, and T. Kato (2001), Estimating source parameters from deformation data, with an application to the March 1997 earthquake swarm off the Izu peninsula, Japan, *Journal of Geophysical Research: Solid Earth*, *106*(B6), 11,217–11,237, doi:10.1029/2000JB900399.

Efron, B., and R. Tibshirani (1986), Bootstrap methods for standard errors, confidence intervals, and other measures of statistical accuracy, *Statistical Science*, *1*(1), pp. 54–75.

Einarsson, P. (1986), Seismicity along the eastern margin of the North American Plate, *The Geology of North America*, *1000*, 99–116.

Einarsson, P. (1991), *Umbrotin við Kröflu 1975–1980 (in Icelandic), in Náttúra Mývatns*, 97-139 pp., Hið Íslenska Náttúrufræðifélag, edited by Árni Einarsson and Arnthór

Garðarsson.

Einarsson, P., and K. Sæmundsson (1987), Earthquake epicenters 1982-1985 and volcanic systems in Iceland: Upptök jarðskjálfta 1982–1985 og eldstöðvakerfi á Íslandi, *Í hlutarins eðli, Fletschrift for Thorbjörn Sigurgeirsson*, edited by Th. Sigfússon.

Ewart, J., B. Voight, and A. Björnsson (1991), Elastic deformation models of Krafla Volcano, Iceland, for the decade 1975 through 1985, *Bulletin of Volcanology*, *53*(6), 436–459, doi:10.1007/BF00258184.

Heap, M., S. Vinciguerra, and P. Meredith (2009), The evolution of elastic moduli with increasing crack damage during cyclic stressing of a basalt from Mt. Etna volcano, *Tectonophysics*, *471*(1–2), 153–160, doi:dx.doi.org/10.1016/j.tecto.2008.10.004, understanding stress and deformation in active volcanoes.

Jónsson, S. (2012), Tensile rock mass strength estimated using InSAR, *Geophysical Research Letters*, *39*(21), doi:10.1029/2012GL053309, l21305.

Kaiser, J. (1953), *Erkenntnisse und Folgerungen aus der Messung von Geräuschen bei Zugbeanspruchung von metallischen Werkstoffen*, Verlag Stahleisen.

Lavrov, A. (2003), The Kaiser effect in rocks: principles and stress estimation techniques, *International Journal of Rock Mechanics and Mining Sciences*, *40*(2), 151–171, doi: 10.1016/S1365-1609(02)00138-7.

Li, C., and E. Nordlund (1993), Experimental verification of the Kaiser effect in rocks, *Rock Mechanics and Rock Engineering*, *26*(4), 333–351, doi:10.1007/BF01027116.

Lockner, D. (1993), The role of acoustic emission in the study of rock fracture, *International Journal of Rock Mechanics and Mining Sciences & Geomechanics Abstracts*, *30*(7), 883 – 899, doi:10.1016/0148-9062(93)90041-B.

Mogi, K. (1958), Relations between the eruptions of various volcanoes and the deformations of the ground surfaces around them, *Bulletin of the Earthquake Research Institute University of Tokyo*, *36*, 99–134.

Okada, Y. (1992), Internal deformation due to shear and tensile faults in a half-space, *Bulletin of the Seismological Society of America*, *82*(2), 1018–1040.

Peltier, A., V. Famin, P. Bachélery, V. Cayol, Y. Fukushima, and T. Staudacher (2008), Cyclic magma storages and transfers at Piton de la Fournaise volcano (La Réunion hotspot) inferred from deformation and geochemical data, *Earth and Planetary Science Letters*, *270*(3–4), 1800–188, doi:10.1016/j.epsl.2008.02.042.

Segall, P. (2013), Volcano deformation and eruption forecasting, *Geological Society, London, Special Publications*, *380*(1), 85–106, doi:10.1144/SP380.4.

Sigmundsson, F. (2006), *Iceland geodynamics: Crustal deformation and divergent plate tectonics*, Springer Science & Business Media.

Simpson, D. W., and S. K. Negmatullaev (1981), Induced seismicity at Nurek reservoir, Tadjikistan, USSR, *Bulletin of the Seismological Society of America*, *71*(5), 1561–1586.

Sturkell, E., F. Sigmundsson, H. Geirsson, H. Ólafsson, and T. Theodórsson (2008), Multiple volcano deformation sources in a post-rifting period: 1989–2005 behaviour of Krafla, Iceland constrained by levelling, tilt and GPS observations, *Journal of Volcanology and Geothermal Research*, *177*(2), 405–417, doi:10.1016/j.jvolgeores.2008.06.013.

Voight, B., R. P. Hoblitt, A. B. Clarke, A. B. Lockhart, A. D. Miller, L. Lynch, and J. McMahon (1998), Remarkable cyclic ground deformation monitored in real-time on

Montserrat, and its use in eruption forecasting, *Geophysical Research Letters*, *25*(18), 3405–3408, doi:10.1029/98GL01160.

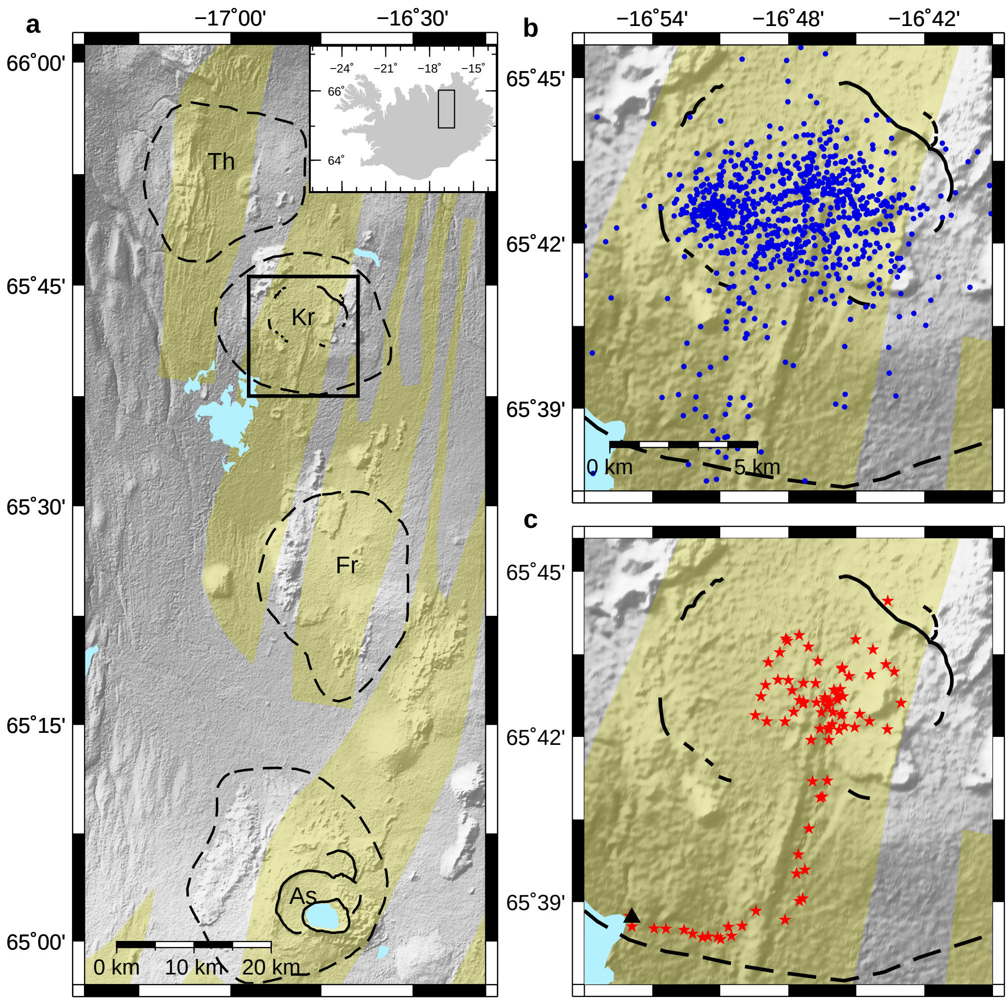

Figure 1. **Krafla: Overview of area and data. a-c** | (a) Volcanic systems of the Northern Volcanic Zone, Þeistareykir (Th), Krafla (Kr), Fremrinámar (Fr) and Askja (As) [*Einarsson and Sæmundsson*, 1987]. Approximate outlines of volcanic systems are denoted by dashed lines, caldera faults by solid lines and fissure swarms are shaded yellow. (b) Located events associated with caldera inflation 1975–1989. (c) Leveling benchmarks (red stars) and location of the seismic station used for earthquake counting (black triangle).

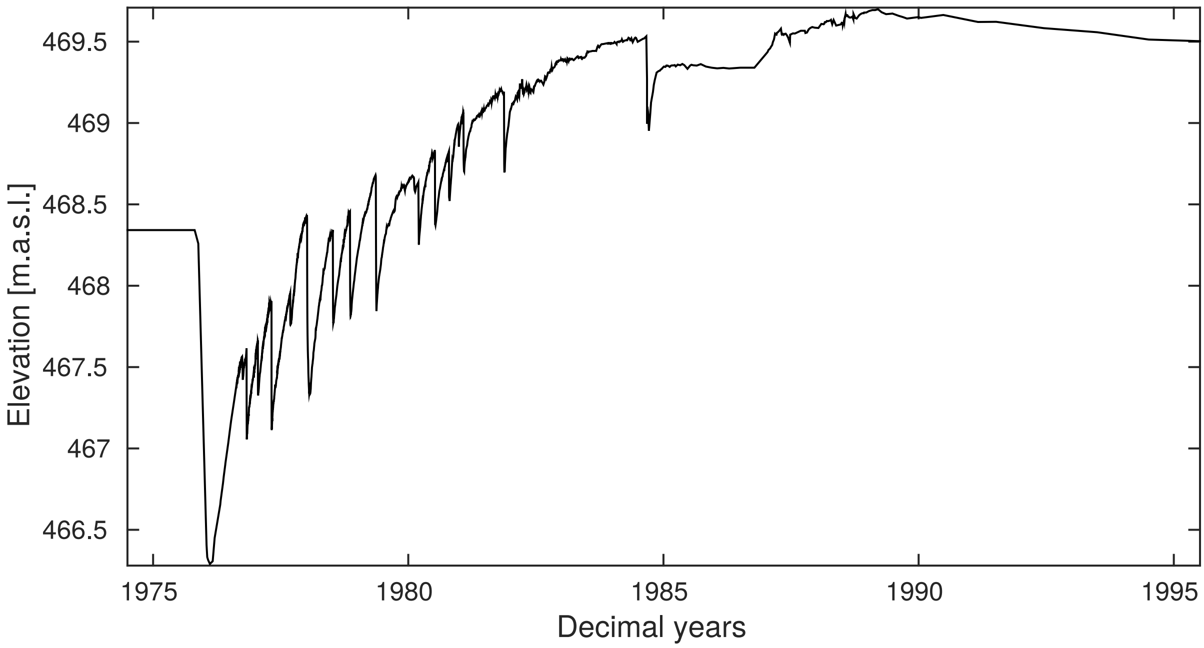

Figure 2. **Example of leveling data time-series** | The elevation changes of benchmark FM5596 were among the greatest for any of the benchmarks used in this study. Interpolation between surveys is based on daily and semi-continuous tilt measurements at one site.

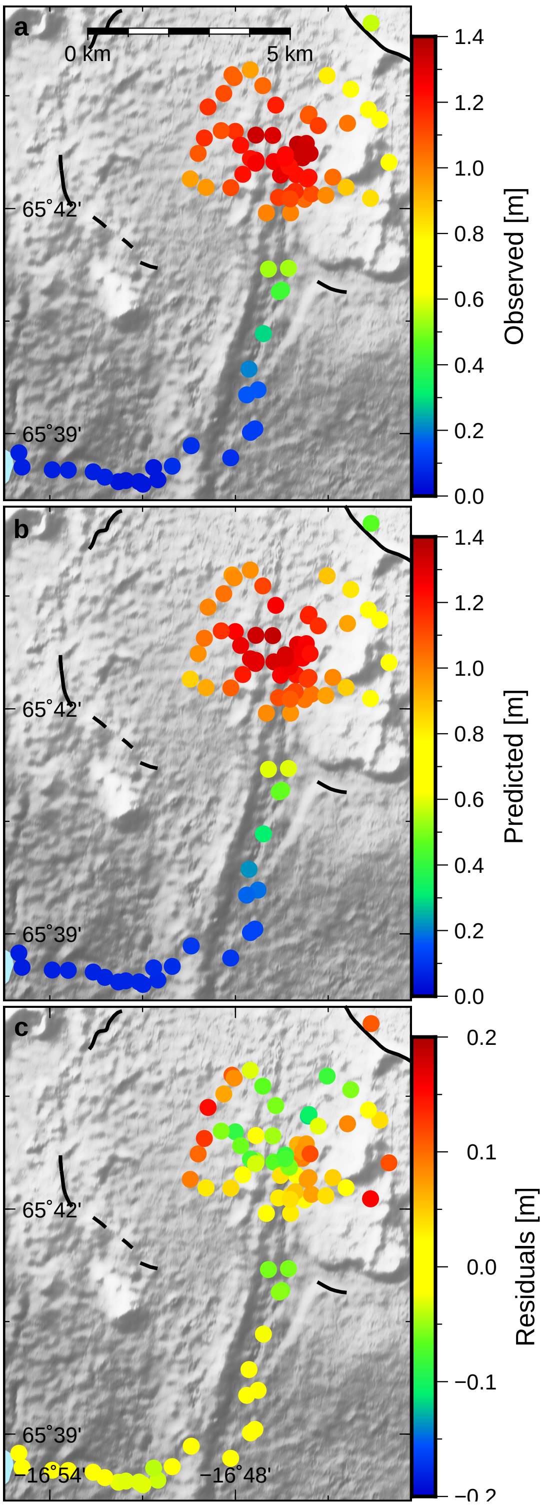

Figure 3. **Example inversion results a-c** | Cumulative vertical displacements on 26 April 1977 (decimal year 1977.3177) a day before the first southward traveling dike. (a) observed vertical displacement u^{obs}, (b) model predicted vertical displacements and (c) the residual: $u^{\mathrm{pre}} - u^{\mathrm{obs}}$. The agreement is good between the observed and model predicted vertical displacement.

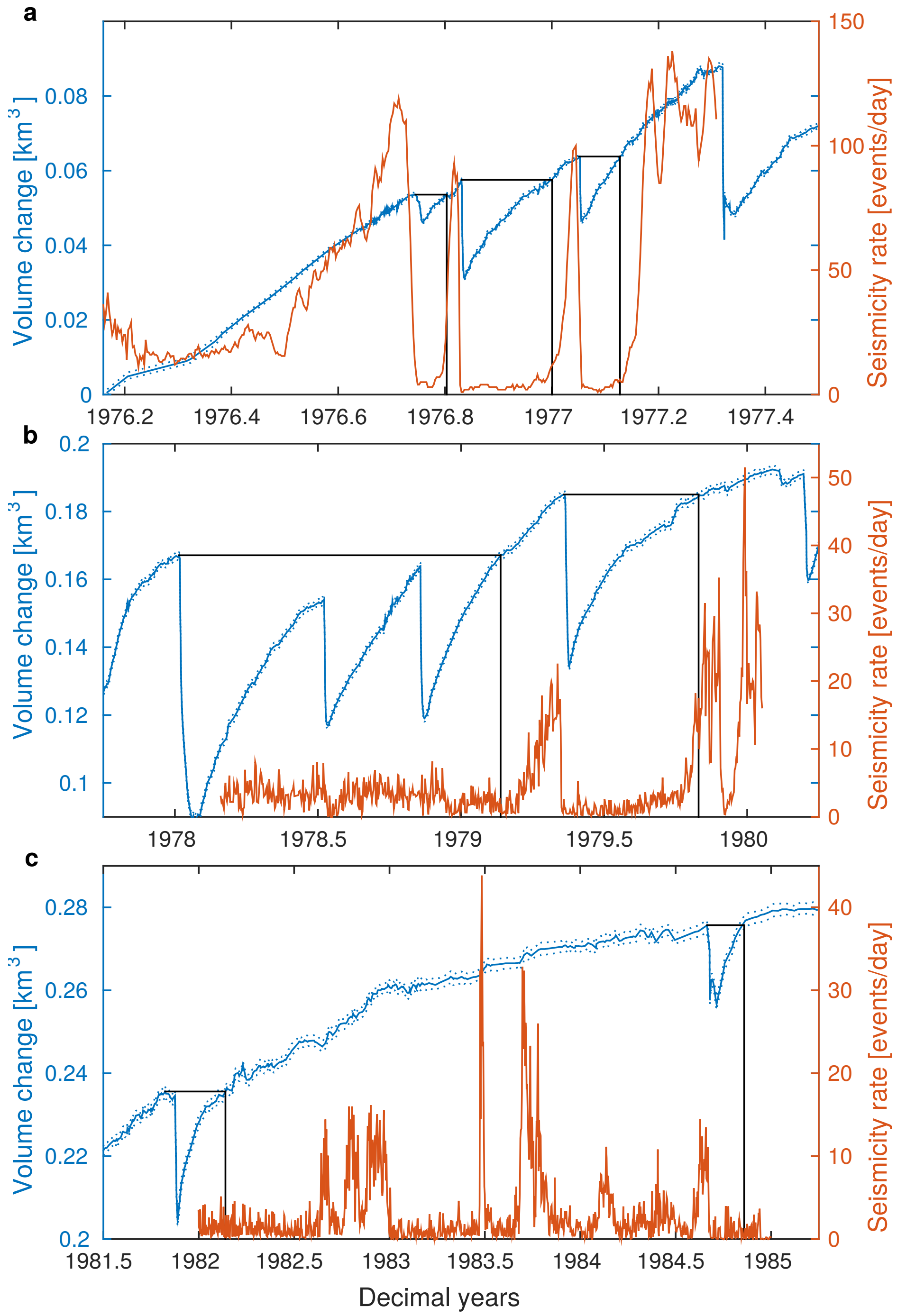

Figure 4. Comparison of seismicity rate and point source volume change a–c| The three panels show the three periods for which caldera inflation seismicity rate data is available. The seismicity rate is a 5-day running mean. Horizontal black lines show maximum inflation of a previous cycle. Vertical black lines are projections of the point where the previous maximum inflation is exceeded onto the time scale. The solid blue volume change line represents the best-fitting model. Dotted lines above and below the volume change line indicate the 95% confidence interval for the volume change.